Title

The impact of deep space radiation on cognitive performance: From biological sex to biomarkers to countermeasures

Journal

Science Advances, 7(42)

ISSN

2375-2548

Authors

Krukowski, Karen
Grue, Katherine
Becker, McKenna
et al.

Publication Date

2021-10-15

DOI

10.1126/sciadv.abg6702

Peer reviewed

NEUROSCIENCE

The impact of deep space radiation on cognitive performance: From biological sex to biomarkers to countermeasures

Karen Krukowski[1,2], Katherine Grue[1,2], McKenna Becker[1,2], Edward Elizarraras[1,2], Elma S. Frias[1,2], Aaron Halvorsen[1,2], McKensie Koenig-Zanoff[1,2], Valentina Frattini[1,2], Hasitha Nimmagadda[1,2], Xi Feng[1,2], Tamako Jones[3], Gregory Nelson[3], Adam R. Ferguson[2,4,5,6], Susanna Rosi[1,2,4,5,7]*

In the coming decade, astronauts will travel back to the moon in preparation for future Mars missions. Exposure to galactic cosmic radiation (GCR) is a major obstacle for deep space travel. Using multivariate principal components analysis, we found sex-dimorphic responses in mice exposed to accelerated charged particles to simulate GCR (GCRsim); males displayed impaired spatial learning, whereas females did not. Mechanistically, these GCRsim-induced learning impairments corresponded with chronic microglia activation and synaptic alterations in the hippocampus. Temporary microglia depletion shortly after GCRsim exposure mitigated GCRsim-induced deficits measured months after the radiation exposure. Furthermore, blood monocyte levels measured early after GCRsim exposure were predictive of the late learning deficits and microglia activation measured in the male mice. Our findings (i) advance our understanding of charged particle–induced cognitive challenges, (ii) provide evidence for early peripheral biomarkers for identifying late cognitive deficits, and (iii) offer potential therapeutic strategies for mitigating GCR-induced cognitive loss.

INTRODUCTION

"We want to explore… We believe in what we're doing. Now it's time to GO."

–Eileen Collins, NASA astronaut

We are rapidly approaching the next era of human exploration, in which we will embark on missions back to the moon and on to Mars. As with previous expeditions, these journeys present new obstacles, including technical, psychological, and physical stressors. One of the largest stressors is exposure to galactic cosmic radiation (GCR) encountered outside of the Earth magnetosphere. GCR is composed of protons, helium nuclei, and high-energy nuclei of other stable elements, which deposit their energy in dense tracks of ionization (*1*). Current estimates suggest that during deep space missions, astronauts will experience 10-fold higher GCR exposure than when on the International Space Station, where astronauts are protected by the Earth magnetosphere. Current calculations show that in deep space, an individual cell will be traversed by protons approximately once every 3 days, helium nuclei once every 3 weeks, and particles of atomic number (Z) $\geq$ 2 once every 3 months (*2*). Given these exposure statistics, it is imperative to understand how GCR will affect astronauts' cognitive and functional capabilities, thereby affecting mission success.

Because of the limited number of individuals who have endured GCR exposure in deep space travel, research has focused on preclinical animal models to understand the effect of simulated GCR exposure (using accelerated charged particles or ions) on cognitive, behavioral, and cellular responses. Studies have identified maladaptive cognitive alterations, including deficits in learning and memory, fear/startle responses, anxiety phenotypes, and social behaviors in mice and/or rats exposed to an individual type of charged particle [reviewed in (*3*)]. A few studies from our group and others have started investigating the compounding effects of multi-ion exposure on cognitive and behavioral outputs (*4*–*6*) to better recapitulate the harsh space environment astronauts will face. These observed maladaptive simulated GCR–induced responses display a sex-dimorphic phenotype, with cognitive and cellular deficits primarily found in male rodents (*4*).

Mechanistically, charged particle–induced behavioral and cognitive deficits are associated with changes in neuronal function and/or structure as well as altered inflammatory responses [reviewed in (*3*)]. Charged particle–mediated inflammatory responses are primarily characterized by enhanced microglia activation shown to be present up to 12 months after exposure (*7*). Microglia are the brain's innate immune cells accounting for 10 to 15% of all cells. Microglia can regulate neuronal function through direct synaptic interaction or indirectly through the release of cytokines that alter neurotransmission (*8*). Microglia can produce inflammatory cytokines and display a phagocytic morphology weeks to months after exposure to single species of the following particles: protons (*5*), helium (*9*–*11*), iron (*12*, *13*), and titanium or silicon ions (*14*) in male rodents. Furthermore, these studies demonstrated that simulated GCR–induced microglia responses can affect neuronal structure and function, thereby leading to maladaptive behavioral and cognitive outcomes [reviewed in (*7*)]. Together, these data suggest that alteration of microglia phenotypes could be a powerful tool for mitigating GCR-induced cognitive and cellular changes during space flight.

[1]Department of Physical Therapy and Rehabilitation Science, University of California, San Francisco, San Francisco, CA, USA. [2]Brain and Spinal Injury Center, University of California, San Francisco, San Francisco, CA, USA. [3]Department of Basic Sciences, Division of Biomedical Engineering Sciences, Loma Linda University, Loma Linda, CA, USA. [4]Department of Neurological Surgery, University of California, San Francisco, San Francisco, CA, USA. [5]Weill Institute for Neuroscience, University of California, San Francisco, San Francisco, CA, USA. [6]San Francisco Veterans Affairs Healthcare System, San Francisco, CA, USA. [7]Kavli Institute of Fundamental Neuroscience, University of California, San Francisco, San Francisco, CA, USA.
*Corresponding author. Email: susanna.rosi@ucsf.edu

Despite the growing investigation of the cognitive and cellular changes associated with individual or combined ion exposure, many outstanding questions remain. Here, we address two of these questions: (i) Can manipulation of microglia phenotypes be used to mitigate simulated GCR–induced cognitive deficits? (ii) Can we uncover predictive biomarkers for identifying simulated GCR–mediated maladaptive cognitive responses? To answer these questions, we investigated behavioral, cognitive, and cellular changes associated with a "simplified 5-ion GCR simulation" exposure on male and female mice. This protocol is one of two NASA-approved simulations of the galactic cosmic ray environment that can be produced by the NASA Space Radiation Laboratory (NSRL) at Brookhaven National Laboratory (BNL) (*15*). The simplified GCR simulation radiation field consists of protons at two energies as well as He, O, Si, and Fe particles at one energy each, in proportions that roughly span the GCR composition and energy spectrum and can be practically delivered sequentially to biological targets while maintaining dose uniformity throughout the sample (see Materials and Methods). For convenience, we will refer to this irradiation protocol as the "GCRsim." We used multivariate principal components analysis (PCA) to identify GCRsim-induced maladaptive responses including spatial learning deficits. We manipulated microglia through an established depletion and repopulation paradigm (*9*) assessing mitigation of the negative effects of deep space radiation. We analyzed early peripheral blood profiles as predictive tools for identifying at-risk individuals for late GCRsim–mediated maladaptive cognitive responses.

RESULTS

PCA of behavioral and cognitive functions after GCRsim exposure

Twenty-four-week-old male and female C57Bl6/J mice were delivered to BNL for GCRsim exposures consisting of 35% (dose fraction) accelerated protons, 1% silicon ions, 18% helium ions, 6% oxygen ions, 1% iron ions, and 39% protons delivered in that order, at total exposures of 0, 50, and 100 centigray (cGy). Following GCRsim exposure, animals were transported to the University of California, San Francisco (UCSF) for behavioral, cognitive, and cellular assessments (Fig. 1).

A series of behavioral and cognitive tests were used to measure sex- and GCRsim-mediated changes in (i) anxiety-like behavior, (ii) sociability, (iii) social memory, (iv) recognition memory, and (v) spatial learning. Anxiety-like behavior was measured at different time points after GCRsim exposure using the elevated plus maze (EPM) (*4*, *16*) and open-field test (*4*). Sociability and social memory were measured by the three-chamber social test (*4*, *17*, *18*). Recognition memory was investigated in the novel object recognition (NOR) task (*4*, *9*, *19*), and spatial learning was measured in the radial arm water maze (RAWM) (*20*). Previous reports from our group and others have identified single-ion or multi-ion accelerated particle exposure impact on anxiety, sociability, social memory, and recognition memory [reviewed in (*3*)]. None of the reported behavioral and cognitive functions have been investigated using the GCRsim outlined above.

Given the multidimensional nature of behavioral and cognitive responses, we examined the relationships between the measured variables using linear and nonlinear PCA to identify sets of covarying behavioral/cognitive variables that self-organized into functionally related groups based on their cross-correlations (i.e., mean-centered, standardized covariance) (*21*). This analysis yielded four orthogonal principal components (PCs), which accounted for 65.9% of the total variance in behavioral and cognitive performance (Fig. 2A and Table 1). The heatmap shows the PC loading weights for variables onto the four PCs; individual variable labels appear in Table 1. According to the PC loading weights, PC1 reflected sociability, PC2 reflected recognition memory, PC3 modeled social learning, and PC4 was indicative of spatial memory. Distinct workflows of linear PCA, nonlinear PCA, and balanced bootstrapping across 1000 iterations yielded similar results, confirming validity and stability with the sample sizes used (Table 1). Minimal differences were noted when comparing the linear, nonlinear, and bootstrapping PC readouts indicative of linearity and appropriate sample size.

The unbiased PC analysis created new synthetic variables (PCs) that are explicitly uncorrelated (orthogonal) to each other, creating distinct comprehensive variables for (i) sociability (PC1), (ii) recognition memory (PC2), (iii) social memory (PC3), and spatial learning (PC4) identified by standardized PC loading coefficients. We then calculated each subjects' weighted composite score on each of the

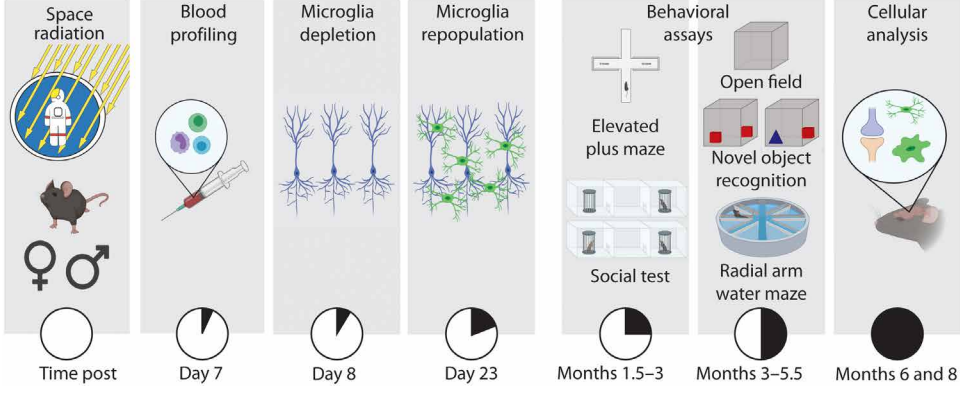

Fig. 1. Experimental design. Six-month-old male and female C57Bl6/J mice underwent GCRsim exposure at BNL. Five days later, animals were shipped to UCSF for additional analysis. One day after arriving at UCSF (7 days after GCRsim exposure), peripheral blood was extracted by tail vein puncture. From days 8 to 23 after exposure, cohorts received microglia depletion chow (PLX5622) or normal chow. From months 1.5 to 5.5, animals underwent behavioral and cognitive testing in the following order: elevated plus maze (EPM), three-chamber social test, open field, novel object recognition (NOR), and radial arm water maze (RAWM). Following behavioral and cognitive testing, animals were euthanized at 6 or 8 months after exposure for microglia or synaptic analysis. Timeline created in BioRender.com.

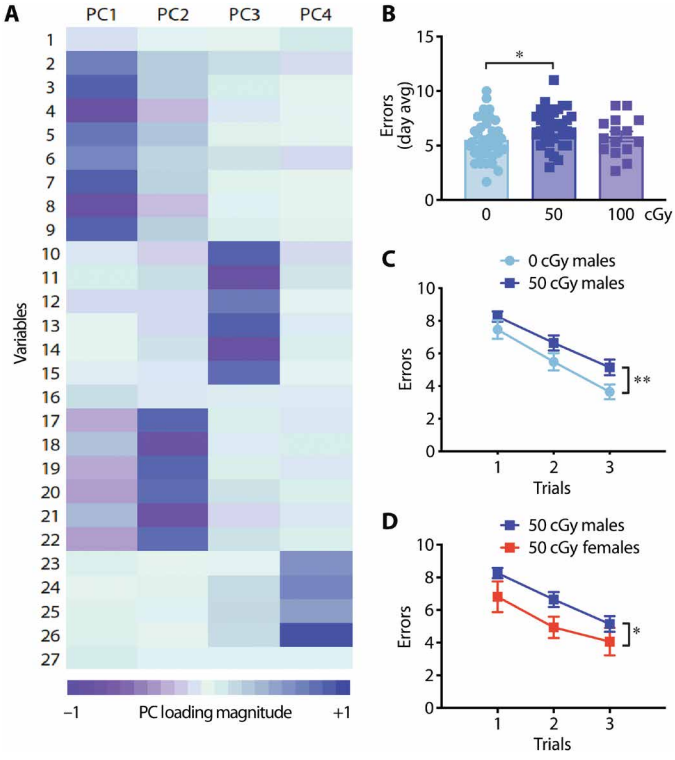

Fig. 2. GCRsim causes sex-dimorphic spatial learning deficits. (**A**) Multidimensional analysis of behavioral and cognitive alterations due to GCRsim exposure was examined using linear PCA. This analysis yielded four orthogonal PCs, which accounted for 65.9% of the total variance in behavioral and cognitive performance: PC1 = sociability, PC2 = recognition memory, PC3 = social memory, and PC4 = spatial memory. Heatmap of PC loading values displayed. Individual variables listed in Table 1. (**B** to **D**) Five months after GCRsim exposure, animals were tested for spatial learning deficits in the RAWM. Male mice exposed to 50 cGy of GCRsim displayed impaired spatial learning deficits when compared to 0 cGy male mice and 50 cGy female mice. (B) The time for all three trials was averaged to calculate an individual mouse score (day average) for 0, 50, and 100 cGy male mice. One-way ANOVA revealed significant differences between groups ($F = 3.76$; $P < 0.05$). Tukey post hoc analysis. (C) Individual trial scores for 0 and 50 cGy male mice. Two-way repeated-measures ANOVA revealed a significant group ($P < 0.01$) and time effect ($P < 0.001$). (D) Individual trial scores for 50 cGy male mice and 50 cGy female mice. Two-way repeated-measures ANOVA revealed a significant group ($P < 0.05$) and time effect ($P < 0.001$). Individual animal scores are represented in dots, and lines depict group mean and SEM. *$P < 0.05$; **$P < 0.01$. *n*: males: 0 cGy = 37; 50 cGy = 34; 100 cGy = 15; females: 50 cGy = 16.

PCs (equivalent to mean-centered *z* scores) and then used these PC scores as primary end point measures for hypothesis testing. Sex- and GCRsim-mediated changes were subsequently investigated within the newly generated four PC variables. General linear modeling [two-way analysis of variance (ANOVA)] identified significant sex-dimorphic performance in sociability (PC1, $P = 0.029$) and recognition memory (PC2, $P = 0.008$). When investigating relationships between sex and GCRsim, sociability and recognition memory displayed trends toward significance ($P = 0.059$ and $P = 0.126$, respectively), and a significant sex by GCRsim interaction was measured in spatial learning (PC4, $P = 0.002$). Next, we further explored sex- and GCRsim-mediated changes in spatial learning.

GCRsim exposure results in sex-dimorphic spatial learning deficits

Spatial learning was measured in the RAWM 5 months after GCRsim exposure. In this forced-swim behavioral test, animals were given three trials to locate a platform hidden under opaque water in one of the eight arms using navigational cues set in the room (*20*). We recorded the total number of entries into the nontarget arms (errors) before the animal found the escape platform with automated tracking software. The number of errors is used as a metric of spatial learning. Male mice exposed to 50 cGy of radiation averaged more errors before finding the escape platform when compared with 0 cGy male mice (Fig. 2, B and C), denoting GCRsim-induced impairments in spatial learning. No impairments were measured in the 100 cGy group. Strikingly, female mice exposed to 50 cGy of radiation did not display impairments in spatial learning when compared with the female 0 and 100 cGy groups (fig. S1A). Furthermore, when compared with male 50 cGy mice, female mice exposed to identical radiation conditions (50 cGy) made fewer errors in the RAWM (Fig. 2D). These data demonstrate sex-dimorphic responses to GCRsim, with only male mice displaying deficits in spatial learning.

Brief microglia depletion mitigates GCRsim-induced learning deficits

We then tested whether brief microglia depletion blocked GCRsim-induced spatial learning deficits. Seven days after GCRsim exposure, mice were switched to PLX5622–1200 ppm (PLX) or control diet for 15 days (Fig. 3A, yellow highlights) (*9*). The PLX diet was composed of a colony-stimulating factor 1 receptor (CSF1-R) inhibitor that depleted microglia within 3 days (~90%) and sustained the depleted state throughout the duration of the 15-day treatment (*22*). Upon returning to a normal diet, microglia repopulation occurs within 7 days (*23*). Spatial learning was measured 5 months after radiation exposure (Fig. 3A, yellow highlights), long after microglia have fully repopulated. Male mice exposed to 50 cGy of radiation and treated with PLX (50 cGy + PLX) showed spatial learning performance indistinguishable from the 0 cGy control mice (Fig. 3B). No differences were observed when comparing the 50 cGy and 50 cGy + PLX groups. Moreover, no differences were measured when comparing female 50 cGy and female 50 cGy + PLX groups; however, the female 50 cGy + PLX group did perform slightly better than the female 0 cGy group (comparison between 0 and 50 cGy + PLX; fig. S1B). These data demonstrate that brief microglia depletion shortly after exposure mitigated deep space radiation–induced late learning deficits measured in male mice.

Temporary microglia depletion decreases phagocytic protein levels and increases complement markers in the repopulated microglia

We next investigated whether the phagocytic activity of the repopulated microglia could be responsible for the PLX-mediated mitigation of spatial learning deficits. Increased phagocytic and complement protein expression on microglia denote an activated and/or inflammatory phenotype (*8*). Thus, we quantified phagocytic proteins and complement molecules on isolated microglia by flow cytometry (fig. S2) (*9*). GCRsim (50 cGy) resulted in an increased expression of two phagocytic markers: CD107a and CD68 at 6 months (Fig. 3, C and D) and 8 months (fig. S3, A and B) after radiation exposure in male mice. We did not observe increases in microglia phagocytic markers (CD107a and CD68) in female mice at 8 months

Table 1. Multivariate analysis of GCRsim-induced maladaptive responses. Multidimensional analysis of behavioral and cognitive alterations due to GCRsim exposure was examined by linear and nonlinear PCA with bootstrapping. This analysis yielded four orthogonal PCs, which accounted for 65.9% of the total variance in behavioral and cognitive performance: PC1 = sociability, PC2 = recognition memory, PC3 = social memory, and PC4 = spatial memory. Variables in the table correspond with the heatmap in Fig. 2. Variables not listed in the table: variable 1 = time in open + center (in seconds) in EPM; variable 16 = time in center (in seconds) in open-field test.

	Linear	Nonlinear	Bootstrapping
PC1: Sociability. Variance explained = 23%, *n* = 189			
Interaction time with mouse (seconds) 3 min (2)	0.707	0.721	0.716
Interaction time with mouse (%) 3 min (3)	0.872	0.868	0.864
Interaction time with empty cage (%) 3 min (4)	−0.872	−0.868	−0.864
Sociability ratio 3 min (5)	0.761	0.859	0.857
Interaction time with mouse (seconds) 5 min (6)	0.666	0.679	0.674
Interaction time with mouse (%) 5 min (7)	0.891	0.876	0.874
Interaction time with empty cage (%) 5 min (8)	−0.891	−0.876	−0.874
Sociability ratio 5 min (9)	0.865	0.874	0.872
PC2: Recognition memory. Variance explained = 18%, *n* = 189			
Interaction time with novel object (%) 3 min (10)	0.849	0.79	0.784
Interaction time with familiar object (%) 3 min (11)	−0.849	−0.79	−0.784
Discrimination index (%) 3 min (12)	0.849	0.79	0.784
Interaction time with novel object (%) 5 min (13)	0.818	0.785	0.779
Interaction time with familiar object (%) 5 min (14)	−0.818	−0.785	−0.779
Discrimination index (%) 5 min (15)	0.818	0.785	0.779
PC3: Social memory. Variance explained = 16%, *n* = 189			
Interaction time with novel mouse (%) 3 min (17)	0.87	0.905	0.896
Interaction time with familiar mouse (%) 3 min (18)	−0.87	−0.905	−0.896
Social memory ratio 3 min (19)	0.742	0.891	0.885
Interaction time with novel mouse (%) 5 min (20)	0.877	0.884	0.874
Interaction time with familiar mouse (%) 5 min (21)	−0.877	−0.884	−0.874
Social memory ratio 5 min (22)	0.812	0.884	0.873
PC4: Spatial learning. Variance explained = 8%, *n* = 189			
Trial 1 errors (23)	0.612	0.807	0.799
Trial 2 errors (24)	0.671	0.506	0.496
Trial 3 errors (25)	0.534	0.356	0.363
Block 1 errors (26)	0.969	0.877	0.866
Trial 1 duration (27)		0.798	0.789

after radiation exposure (fig. S3, C and D). The repopulated microglia from male mice (50 cGy + PLX group) showed a significant decrease of CD107a and CD68 levels when compared to the 50 cGy group (Fig. 3, C and D). CD107a and CD68 levels in the 50 cGy + PLX group were indistinguishable from the 0 cGy group. GCRsim exposure resulted in an increased microglia phagocytic marker chronically (up to 8 months after GCRsim exposure), while temporary microglia depletion months earlier reset the GCRsim-induced phagocytic increases.

Microglia expression levels of two mediators of the complement pathway, C5aR1 and CD11b (CR3A), were then characterized. Repopulated microglia from the 50 cGy + PLX group had increased C5aR1 levels when compared with both the 0 and 50 cGy groups (fig. S3A). No changes in microglia C5aR1 or CD11b protein levels were measured when comparing the 50 cGy and 0 cGy groups at 6 months (fig. S4, A and B) or 8 months (fig. S4, C and D) after radiation exposure. Increased CD11b levels were measured when comparing the 50 cGy + PLX and 0 cGy groups (fig. S4B). These data suggest that exposure to GCRsim alone does not alter microglia complement protein expression levels; however, brief microglia depletion followed by repopulation can modestly affect microglia complement expression levels measured months later.

We did not observe any differences in microglia raw numbers ($CD11b^{+}CD45^{low}$) when comparing the different treatment groups (fig. S5A), in line with our previous report (*9*). We measured GCRsim-induced increases in CD45 protein levels at 6 months (fig. S5B) that resolved by 8 months after exposure (fig. S5C). Brief microglia depletion blocked CD45 protein level increases (fig. S5B). These data demonstrate that GCRsim exposure results in long-term microglia activation as measured by increased phagocytic molecules

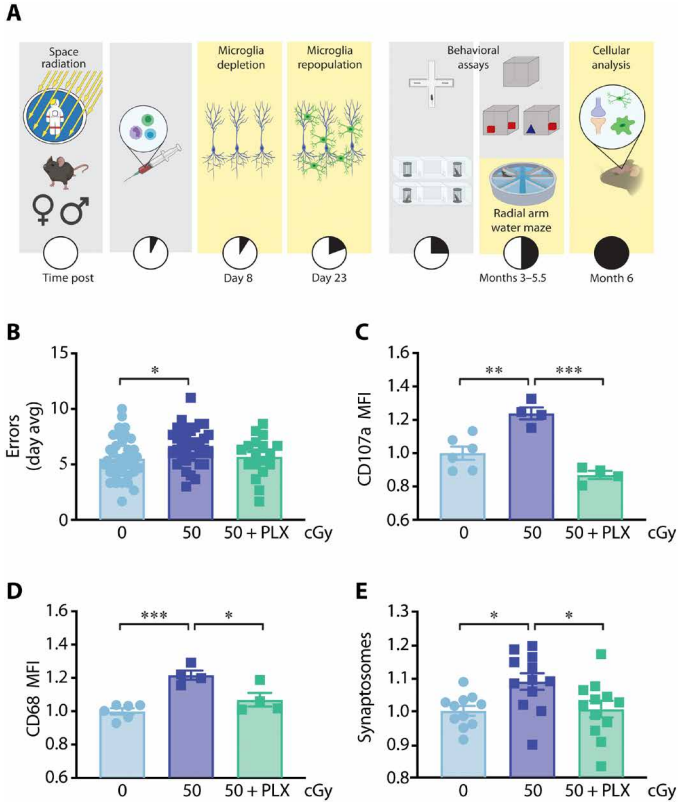

Fig. 3. Brief microglia depletion mitigates deep space radiation–induced learning deficits, microglia phagocytic activation, and synaptic levels. (**A**) Experimental design (see Fig. 1): Yellow highlights denote experimental design steps discussed in this figure. (**B**) Male mice exposed to 50 cGy + PLX were protected from GCRsim-induced spatial learning deficits. Day averages for 0 cGy, 50 cGy, and 50 cGy + PLX male mice. One-way ANOVA revealed significant differences between groups ($F = 3.96$; $P < 0.05$). Tukey post hoc analysis. Individual animal scores are represented in dots, and lines depict group mean and SEM. (**C** and **D**) Hemibrains were collected for flow cytometric analysis of microglia at 6 months after radiation exposure. MFI was used to compare the phagocytic protein levels in microglia populations ($CD11b^{+}CD45^{low}$) of 0 cGy, 50 cGy, and 50 cGy + PLX male mice. Microglia depletion blocked GCRsim-induced increases in (C) CD107a and (D) CD68 protein levels. (C) One-way ANOVA revealed significant differences between groups ($F = 22.16$; $P < 0.0001$). Tukey post hoc analysis. (D) One-way ANOVA revealed significant differences between groups ($F = 15.68$; $P < 0.001$). Tukey post hoc analysis. Individual animals are represented in dots, and lines depict group mean and SEM. Males *n*: 0 cGy = 6; 50 cGy = 4; 50 cGy + PLX = 4. (**E**) Hippocampal synaptosomes were isolated by sucrose gradient and first determined by size calibration beads and then coexpression of pre- and post-synaptic markers. Pre-synaptic marker, synapsin-1; post-synaptic marker, PSD-95. Temporary microglia depletion mitigates GCRsim-mediated increased synapses. One-way ANOVA revealed significant differences between groups ($F = 4.88$; $P < 0.05$). Tukey post hoc analysis. Individual tubes are represented in dots, and lines depict group mean and SEM. Males *n*: 0 cGy = 11; 50 cGy = 12; 50 cGy + PLX = 12. $^{*}P < 0.05$; $^{**}P < 0.01$, $^{***}P < 0.001$.

without affecting microglia numbers. Brief depletion of microglia shortly after radiation exposure blocked chronic microglia activation.

Temporary microglia depletion blocks GCRsim-induced changes in synapse number

Microglia can regulate neuronal function through direct interaction with synapses (*24*); therefore, we next investigated whether PLX-mediated microglia alterations affected synapse number. We measured synaptic number by flow synaptocytometry (*4*), a technique that allows for labeling and quantification of synapses from isolated brain regions (fig. S6). Male mice exposed to 50 cGy of GCRsim had significantly more hippocampal synapses when compared to the 0 cGy group (Fig. 3E). Temporary, acute microglia depletion blocked GCRsim-induced synaptic increases (comparison between 50 cGy and 50 cGy + PLX; Fig. 3E). Moreover, the synapse numbers in the 50 cGy + PLX group were indistinguishable from the 0 cGy group, denoting complete reversal of GCRsim-induced phenotypes. These data demonstrate that GCRsim exposure results in an aberrant increase in synapses that can be prevented by temporary microglia depletion. The aberrant synapse increase could be responsible for the memory deficits measured.

Predictive peripheral biomarker of GCRsim-induced deficits

Identifying early blood biomarkers predictive of GCRsim-induced cognitive and behavioral deficits could be critical for mission success. We investigated whether the percentages of peripheral blood cell populations measured acutely after radiation exposure covaried with behavioral and cognitive impairments measured months later. Peripheral blood was extracted 1 week after radiation exposure and screened by flow cytometric analysis for percentages of peripheral immune cells (Fig. 4A, highlighted in yellow). Exposure to 50 cGy of GCRsim increased peripheral monocyte percentages in both male (Fig. 4B) and female mice (fig. S7A) when compared with sex-matched 0 cGy groups. To determine the functional relevance for using acute blood monocyte percentages as a predictive biomarker for GCRsim-induced cognitive deficits, the individual spatial learning performance of each mouse (block 1 errors) was plotted against its specific percentage of monocytes in the blood. We measured a significant, positive correlation between acute blood monocyte percentages and chronic spatial learning in male mice (Fig. 4C). This positive correlation was also observed when PC4 (spatial learning generated PC, see Table 1) was plotted against acute peripheral monocyte levels (Pearson correlation = 0.439, $P = 0.01$). No relationships were measured between blood monocyte percentages and spatial learning performance in female mice (fig. S7B). These data further enhance the potential for using peripheral immune cell percentage changes as predictive biomarkers for long-term impairments in male mice.

Multidimensional pattern of GCRsim-induced alterations

To better understand the multidimensional sequelae of GCRsim radiation exposure in male mice, we performed integrative data–driven analysis in a cohort of subjects with multiple measures: (i) spatial learning, (ii) microglia activation, and (iii) peripheral monocyte levels assessing the global pattern of biobehavioral correlations reflecting syndromic (*25*) alterations. To directly assess cross-modality covariance, we performed PCA on the full set of end points from the same subjects. We plotted the interrelationship of these variables using the syndRomics package (Fig. 4D), which represents loadings as weighted vectors. The results demonstrate that exposure to GCRsim generates a coherent pattern of dysfunction across behavioral and biological variables accounting for 64% of the total variance across measures. Specifically, microglial activation and phagocytic profiles were associated with increased blood monocyte markers and spatial learning deficits.

Overall, the multidimensional analyses allowed us to distill the complex set of inflammatory interrelationships into a single composite

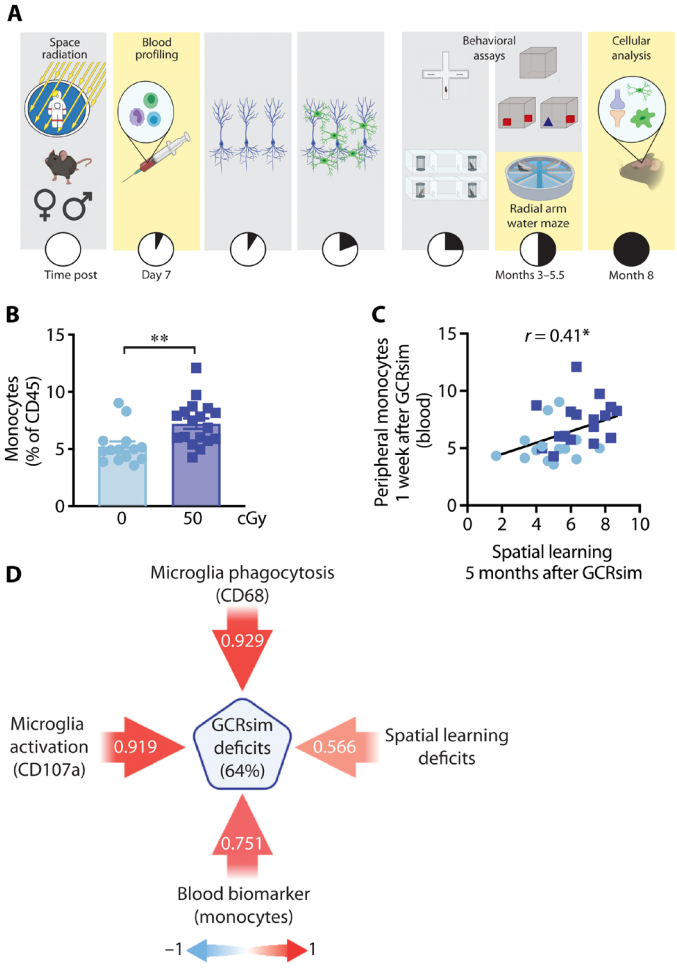

Fig. 4. Predictive peripheral biomarker of GCRsim-induced deficits. (**A**) Experimental design: Animals were exposed to GCRsim; 7 days later, peripheral blood was extracted by tail vein puncture on awake animals. From 5 to 5.5 months after radiation exposure, animals were tested for spatial learning deficits in RAWM. At 8 months after radiation exposure, animals were terminated and tissues were collected for analysis. Yellow highlights denote experimental design steps discussed in this figure. (**B**) Seven days after GCRsim exposure, blood was extracted by a tail vein bleed on awake animals. Peripheral immune cell populations were assessed by flow cytometry. Peripheral monocytes identified by $CD45^+$, $CD11b^+$, $Ly6G^-$, $CD4^-$, $CD8^-$. Male mice exposed to 50 cGy of GCRsim had increased peripheral monocyte percentages 1 week after exposure. Data represent the percentage of monocyte cells within the $CD45^+$, $Ly6G^-$ leukocyte population. Student's *t* test. Individual animal scores are represented in dots, and lines depict group mean and SEM. $^{**}P < 0.01$. (**C**) A linear regression model was used to investigate relationships between spatial learning and acute monocyte percentages to determine predictive potential of blood biomarkers. A positive correlation was measured between spatial learning at 5 months after exposure (*x* axis) and percentage of peripheral monocytes 1 week after exposure (*y* axis), $r = 0.41$, $P = 0.01$. Light blue circles, 0 cGy; dark blue squares, 50 cGy. *n*: males: 0 cGy = 14; 50 cGy = 18. (**D**) Multivariate analysis of GCRsim-induced changes in (i) blood monocyte levels, (ii) microglia activation/phagocytosis, and (iii) spatial learning was measured by PCA, resulting in 1 PC that accounted for 64% of the variance. PC1, denoted as GCRsim deficits, is depicted with individual variable variances depicted. Strong relationships between blood monocyte, microglia activation, and spatial learning were observed.

pattern that better predicted spatial learning deficits than each of the individual biomarkers on their own (e.g., compare $r = 0.41$ Pearson in Fig. 4C with $r = 0.57$ loading in Fig. 4D). The multidimensional effects of microglial and monocyte biomarkers together accounted for 64% of the total variance across these biobehavioral associations. Together, this argues that multidimensional inflammatory biomarkers are strong predictors of outcome after GCRsim.

DISCUSSION

Here, we cement the essential role of microglia activation in space-like radiation (GCRsim)–induced cognitive decline in male mice. Furthermore, we identify a therapeutic (PLX) for mitigation of the radiation-induced spatial learning deficits. Last, we found that peripheral blood monocyte levels can be used as an early biomarker for predicting long-term GCRsim-mediated microglia activation and cognitive decline in male mice. In line with our previous study that used different ion composition exposure (*4*), a sex-dimorphic response was measured: All deficits were observed in male mice, with female mice protected from GCRsim-induced phenotypes, as summarized in Fig. 5.

We identify GCRsim-induced deficits in spatial learning using composite PC scores (optimally weighted *z* scores) derived by manifold machine learning as primary end points. Spatial learning refers to an organism's ability to encode information about their environment and to use this information to navigate through it. As astronauts will traverse unknown terrain on a Mars mission, deficits in this cognitive modality would greatly impair mission success. We found that brief microglia depletion shortly after exposure mitigates long-term GCRsim-induced deficits in spatial learning, suggesting that while deep space radiation exposure could impair spatial learning, there are tools that can alleviate these deficits. We did not observe deficits in other behavioral (anxiety-like and sociability) or cognitive (social memory and recognition memory) paradigms. Previous findings have shown that charged particle exposure causes deficits in one or more of these measured domains (*9*, *13*, *14*, *18*, *26*–*28*); however, the current data demonstrate that when combined, the five ions might have different combinatory effects that are not cumulative. While space radiation is the prominent stressor for deep space journeys, there are additional aggravating factors that might affect astronauts, including social isolation, zero gravity, distance from earth, hostile environment, and altered sleep patterns (*29*). Determining whether the combination of these stressors with GCRsim exposure affects behavioral and cognitive function is a crucial next step for mission preparation.

Biomarkers will be extremely important during extended space missions due to constantly changing conditions and limited personnel. Detecting impending maladaptation or functional impairment provides an opportunity for intervention before consequences become severe or irreversible. Here, we found that monocyte percentages measured 1 week after GCRsim exposure were predictive of long-term spatial learning deficits measured 5 months later in male mice. These data suggest that blood monocyte levels could be used as a predictive biomarker for long-term deficits. While other studies have investigated blood immune changes due to deep space radiation exposure in humans (*30*) and mice (*31*–*35*), the links with behavioral and cognitive outputs have not been addressed. Our previous report identified relationships between oxygen ion–induced changes in social behaviors and blood T cell levels (*18*). This

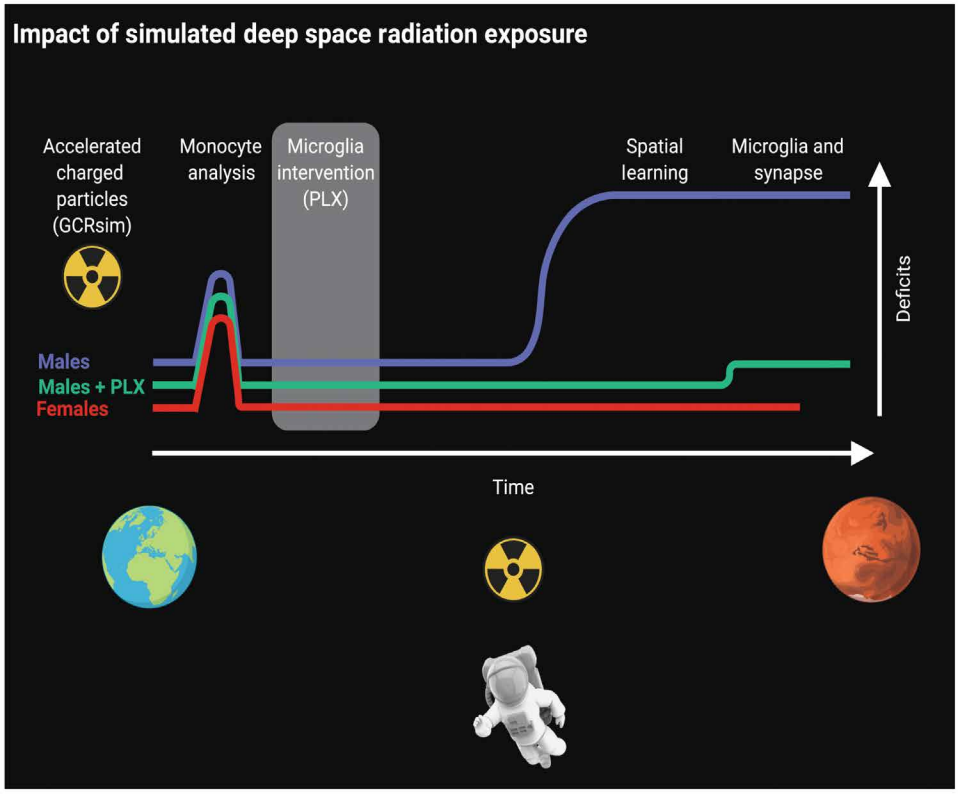

Fig. 5. Impact of simulated deep space radiation exposure. Alluvial diagram to depict the impact of simplified GCRsim over time during future lunar and Mars missions. Male cohorts displayed increased monocyte level, impairments in spatial learning, increased microglia activation, and altered synapse levels. Despite early increased monocyte levels measured in the male + PLX cohort, most other GCRsim impairments were not observed (only minor microglia changes were observed). Female mouse cohorts displayed increased monocyte levels with no other GCRsim impairments. Male mouse cohort is denoted by the blue line, male + PLX cohort (received microglia depletion agent) is denoted by the green line, and female mouse cohort is denoted by the red line. The *x* axis denotes time, and the *y* axis denotes GCRsim-induced decrements. Measurements depict time of assay: (i) Monocyte levels in tail vein blood analyzed by flow cytometric analysis. (ii) PLX administration—microglia depletion agent administered in the chow. (iii) Spatial learning was analyzed by the RAWM. (iv) Microglia and synapse decrements were analyzed by flow cytometry and flow synaptocytometry, respectively. Synapse analysis was not performed on female rodents.

previous study demonstrates a clear link between blood immune populations and behavioral paradigms measured; blood samples were collected postmortem, so it was unclear whether oxygen ion–induced changes occurred before measurement of behavioral changes. Here, we found that monocyte levels are altered months before spatial learning deficits are measured. This observation opens the possibility for the development of predictive modeling of cognitive deficits based on blood biomarkers. The predictive potential of monocytes was only observed in male mice; the increased monocyte numbers measured in female were not predictive of altered spatial learning. In this study, we only investigate monocyte levels at a single time point after radiation exposure; additional analysis is needed to determine the duration of altered monocyte levels and sex-dimorphic biomarker responses. The integrative multidimensional associations we developed here provide initial weights that may be further developed through confirmatory theoretical models in the future.

Individual accelerated ion exposure affects microglia function and morphology (*7*). Previous reports have identified increased microglia numbers or activation levels primarily through immunofluorescence imaging (Iba-1, CD68), finding increased numbers/levels throughout the brain with particular focus on vulnerable regions such as the hippocampus [reviewed in (*3*, *7*)]. Here, we find that GCRsim exposure induced long-term changes in microglia activation in male mice at both 6 and 8 months after irradiation. Microglia activation was measured by increased CD68 and CD107a (Lamp1) protein levels. CD68 and CD107a are predominantly expressed in lysosomes and are widely used as markers of microglia phagocytic activity (*8*). Brief microglia depletion (1 week after GCRsim exposure with PLX) followed by microglial repopulation mitigated the GCRsim-induced phagocytic phenotype; CD68 and CD107a protein levels return to levels indistinguishable from unirradiated animals. These data demonstrate that early manipulation of microglia after GCRsim exposure can modulate microglia phenotypes months later. This phenomenon of modulating GCR-induced microglia responses briefly after radiation exposure was first demonstrated (by our group) with helium ion irradiation (*9*). Later, a second study by an independent group found that continuous microglia depletion also prevented helium ion–induced cognitive changes (*11*). Here, we have shown that this same treatment paradigm is effective in reversing spatial memory deficits and microglia changes induced by a more complex GCR simulation paradigm.

GCRsim exposure resulted in an increased number of synapses in the hippocampus of male mice; synapse levels were not measured

in female mice. Increased synapse levels were reversed by brief microglia depletion (by PLX) shortly after GCRsim exposure. Previously, we found that triple-ion radiation exposure caused decreased excitatory synapse levels in male mice only that corresponded with (i) increased anxiety-like phenotypes, (ii) decreased social behaviors, and (iii) reduced recognition memory (*4*). While synapse decreases can depend on increased phagocytic activity by microglia (*4*, *9*, *36*), an aberrant increase in synapses can also be associated with maladaptive microglia engulfing capacity (*37*). Together, these results suggest that the response of the brain to GCR is not linear and that GCRsim can affect different cognitive modalities in different ways: Increased synapse levels are associated with spatial learning decrements (as shown here), whereas decreased synapse levels correspond with increased anxiety, reduced social behaviors, and impaired recognition memory (*4*). Additional studies on space radiation–induced synaptic alterations are needed to further define these changes, including additional analysis of females.

In this study, we used a new space radiation field model: simplified five-ion GCR simulation. This irradiation protocol incorporates two additional ions (silicon and iron) from our previously used triple ion (protons, helium, and oxygen) paradigm (*4*) and includes multiple proton exposures to emulate the more frequent interaction of this most abundant component of GCR (*15*). We measured cognitive, cellular, and molecular changes in male mice exposed to 50 cGy of GCRsim. Male mice exposed to 100 cGy of GCRsim did not display spatial learning deficits. This "inverted U-shaped" dose response in which GCRsim-induced alterations is seen only at lower doses and has been observed in other studies (*5*, *9*, *18*, *38*, *39*). Current exposure estimates for the Mars missions are 30 to 45 cGy (*2*, *15*), suggesting that deficits observed here could also occur during future deep space missions. Thus, cellular and molecular changes in the 100 cGy group were outside the scope of this study. However, the GCRsim protocol used here was not a chronic exposure as one would obtain in space, and dose rate effects are currently unknown.

Interplanetary space travel is the exciting next step for human exploration. Despite many unknowns and difficult obstacles, it is clear that deep space travel is imminent. Understanding how the harsh environment of deep space can affect behavioral and cognitive outputs is critical for optimizing mission success. Our findings (i) use multivariate PC analysis to identify GCRsim-induced maladaptive responses including spatial learning deficits, (ii) validate a mitigation strategy for GCR-induced changes, and (iii) provide evidence for a peripheral biomarker as a means for identifying impaired cognitive function.

MATERIALS AND METHODS

Animals

All experiments were conducted in accordance with the National Institutes of Health *Guide for the Care and Use of Laboratory Animals* and were approved by the Institutional Animal Care and Use Committee of UCSF (protocol number, AN18139) and BNL (Upton, NY). Male and female C57Bl6/J wild-type 24-week-old mice were purchased from the Jackson Laboratory and the National Institute on Aging and directly delivered to BNL. Animals underwent simplified five-ion GCRsim exposure at the NSRL—specifics described below. Following GCRsim exposure, animals were transported to UCSF for behavioral and cellular analysis (Fig. 1). At UCSF, animals were housed on a reverse light cycle and environmentally controlled conditions (12:12-hour light:dark cycle at 21 ± 1°C; ~50% humidity)—all had access to food and water ad libitum. When aggressors were identified, they were individually housed with extra enrichment. Chlorhexidine Flush 0.2% Solution (Ceva, Lenexa, KS) was used to treat any wounding that occurred. Mice in which wounding persisted were excluded from analysis. Limited alterations in health states were measured across multiple cohorts and groups with no significant differences due to sex, diet, or GCRsim exposure (table S1). Male and female mice were housed in the same room in groups of one, two, three, or four. Estrous cycles were not monitored.

GCRsim

Following 1 week of acclimation at BNL, mice were then irradiated at the NSRL (*40*) using the NASA-approved simplified GCRsim protocol—five charged particle species delivered in rapid succession to simulate the space radiation spectrum expected inside a deep space vehicle with self-shielding by the human body (*2*, *15*, *41*). These particles were, in order of delivery, 1000 MeV/n protons [linear energy transfer (LET) = 0.20 keV/μm], 600 MeV/n silicon ions (LET = 50.4 keV/μm), 250 MeV/n helium ions (LET = 1.60 keV/μm), 350 MeV/n oxygen ions (LET = 20.9 keV/μm), and 250 MeV/n protons (LET = 0.40 keV/μm), in dose proportions of 35% protons (1000 MeV):1% silicon:18% helium, 6% oxygen, 1% iron, and 39% protons (250 MeV). Total doses of 50 cGy were delivered as part of experimental campaigns NSRL 18B, NSRL 19A, and NSRL 19C, while 100 cGy doses were delivered as part of campaign NSRL 19A. At BNL, animals were housed in groups of four on a normal 12:12 light cycle and transported to the NSRL many hours before GCRsim exposure. Several hours after irradiation, animals were returned to the animal care facility. During each exposure, mice were loaded into 7.3 cm by 4.0 cm by 4.0 cm polystyrene restraint boxes with air holes and mounted on the beam line in cutouts in a standard foam holder. The irradiation time was during the light phase of the circadian cycle. The beam "spot" size was either 20 cm by 20 cm or 60 cm by 60 cm, and animals were placed in the center of the field to assure best uniformity. Over the three NSRL campaigns, the measured doses for the eight 50 cGy exposures were 50.039 ± 0.023 cGy delivered over 15.87 min for 20 cm by 20 cm beams or 46.12 min for the 60 cm by 60 cm beams, yielding dose rates of 3.17 cGy/min or 1.09 cGy/min, respectively. For the two 100 cGy exposures, the measured doses were 100.003 ± 0.002 cGy delivered over an average of 133.2 min for a dose rate of 0.75 cGy/min. The measured proportions of individual ions were as described above, and the maximum deviation from the desired dose contribution was 3% (i.e., 1.03% delivered dose versus 1.00% requested dose) in the case of iron ions. After irradiation, the animals were returned to their home cages and returned to the animal care facility for shipment to UCSF by World Courier within 5 days.

Behavioral analysis

Animals were handled to habituate to investigators and room settings for 1 week before testing. Behavioral assays were performed in dark rooms during the animals' wake cycle. All behavioral equipment was cleaned with 70% ethanol cleaning solution between each animal. All assays were recorded using an overhead camera connected to a video tracking and analysis system (EthoVision XT 12.0, Noldus Information Technology). A combination of EthoVision

software analysis and scoring manually by two investigators blinded to GCRsim and treatment was used for analysis. A subset of videos was scored by EthoVision and manually scored for cross-validation to ensure reliability between computer analysis and manual scoring. All behavioral analysis was performed by one male and four female investigators blinded to the irradiation group. Because of the large animal numbers, it took several weeks to complete all the behavioral assessments; animals were randomized by sex and group over the testing period. No differences between investigators, time of day, or testing window were observed.

Anxiety

One and a half months after GCRsim exposure, the EPM was used to evaluate anxiety-like behavior. The EPM apparatus contains two exposed open arms (35 cm) opposite each other and two enclosed arms (30.5 cm) also across from one another. The arms were attached at a center platform (4.5 cm^2) creating the "plus" shape. The entire apparatus was elevated 40 cm off the floor. Bright white lights were used to illuminate the open arms (*4*, *16*). Individual mice were placed onto the center of the maze and allowed to explore the maze for 5 min while their activity was recorded. The time in the open arm + center was measured (in seconds). Animals that fell from the apparatus, where software errors occurred, or died during the study were excluded from analysis (males: 0 cGy $n = 2$, 0 cGy + PLX $n = 0$, 50 cGy $n = 7$, 50 cGy + PLX $n = 4$, 100 cGy $n = 3$; females: 0 cGy $n = 9$, 0 cGy + PLX $n = 3$, 50 cGy $n = 1$, 50 cGy + PLX $n = 2$, 100 cGy $n = 1$). No significant group outliers were calculated.

Anxiety-like behavior was later measured by the open-field test at ~3 months after GCRsim exposure. For this task, animals were allowed to freely explore an open-field arena (30 cm by 30 cm) for 10 min under red lighting. Activity was recorded, and anxiety-like behavior was calculated by alterations in time spent (in seconds) in the center (17 cm by 17 cm) of the arena. Significant group outliers and animals that died or no longer had whiskers were excluded from analysis (males: 0 cGy $n = 0$, 0 cGy + PLX $n = 0$, 50 cGy $n = 2$, 50 cGy + PLX $n = 4$, 100 cGy $n = 0$; females: 0 cGy $n = 5$, 0 cGy + PLX $n = 0$, 50 cGy $n = 1$, 50 cGy + PLX $n = 0$, 100 cGy $n = 7$).

Sociability and social memory

The three-chamber social approach task was used to test sociability and social memory ~2 to 3 months after GCRsim exposure (*4*, *17*, *18*). Individual animals were placed into a three-chamber arena (72 cm by 50 cm; each chamber is ~24 cm by 50 cm) in a dark room under red light, and behavior was recorded through three consecutive stages: habituation, sociability, and social memory. The habituation phase consisted of 10 min of free exploration. Sociability was measured by placing an empty cage (10 cm in diameter) into one chamber of the arena, and on the opposite side, a stranger age- and sex-matched mouse was placed into a cage—cages were approximately 30 cm apart. Animals were allowed to freely explore the arena for 10 min. The experimental mouse's sociability was measured by their preference for interaction with the mouse rather than the empty cage. Interaction was determined as the nose point of the mouse in close proximity (<5 mm) from the respective cage. Placement of a stranger mouse into the right or left chamber was alternated for each trial. Social memory was measured immediately following the sociability phase as follows—a novel (sex- and age-matched) mouse was placed into the previously empty cage, and social memory was measured by the experimental animal's preference for the novel mouse over the familiar mouse encountered during the sociability phase. During social memory, the experimental mouse interaction was measured for 5 min. Stranger/novel mice consisted of two cages (four mice per cage) of nonaggressive, sex- and age-matched nonlittermate mice. Investigators took extreme caution during testing to avoid odor mixing during testing (cleaning, changing gloves, etc.). All four mice were used in all groups, and no aversions were noted.

Calculated readouts for sociability included (for the first 3 and 5 min of testing) (i) interaction time with mouse (seconds), (ii) interaction time with mouse (%) = ((time of nose interaction with mouse)/(total time of nose interaction with mouse + empty cage)) × 100, (iii) interaction time with empty cage = ((time of nose interaction with empty cage)/(total time of nose interaction with mouse + empty cage)) × 100, and (iv) sociability ratio = (interaction time with mouse (%))/(interaction time with empty cage (%)). Significant group outliers, software issues, and animals that died or no longer had whiskers were excluded from analysis (males: 0 cGy $n = 4$, 0 cGy + PLX $n = 1$, 50 cGy $n = 2$, 50 cGy + PLX $n = 2$, 100 cGy $n = 0$; females: 0 cGy $n = 5$, 0 cGy + PLX $n = 1$, 50 cGy $n = 1$, 50 cGy + PLX $n = 0$, 100 cGy $n = 7$).

Calculated readouts for social memory included (for the first 3 and 5 min of testing) (i) interaction time with mouse (seconds), (ii) interaction time with mouse (%) = ((time of nose interaction with novel mouse)/(total time of nose interaction with novel mouse + familiar mouse)) × 100, (iii) interaction time with familiar mouse = ((time of nose interaction with familiar mouse)/(total time of nose interaction with novel mouse + familiar mouse)) × 100, and (iv) social memory ratio = (interaction time with novel mouse (%))/(interaction time with familiar mouse (%)). Significant group outliers, software issues, and animals that died or no longer had whiskers were excluded from analysis (males: 0 cGy $n = 2$, 0 cGy + PLX $n = 1$, 50 cGy $n = 1$, 50 cGy + PLX $n = 4$, 100 cGy $n = 0$; females: 0 cGy $n = 8$, 0 cGy + PLX $n = 1$, 50 cGy $n = 0$, 50 cGy + PLX $n = 0$, 100 cGy $n = 3$).

Novel object recognition

The NOR assay was used ~3 to 4 months after exposure to measure hippocampal-dependent memory function (*4*, *9*, *19*). A 30 cm by 30 cm by 30 cm arena was used under red lighting for all phases of NOR testing. On the first 2 days, animals freely explored the arena for 10 min per day (habituation phase). On day 3, two identical objects (Duplo red blocks) were secured to the bottom of the arena with magnets in opposite corners (training phase). Mice were given 5 min to freely explore the objects. On day 4, one of the identical objects was replaced by a novel object (Duplo orange flower) of similar size and texture (testing phase). Mice were given 5 min to freely explore the objects. Trials were recorded, and exploratory behavior was defined as time the animals spent directing its nose toward an object. Data are expressed as percent of time mice spent exploring each object. Mice that had <5 s of exploration time during either training or testing were excluded from analysis. In addition, significant group outliers, software issues, and animals that died or no longer had whiskers were excluded from analysis (males: 0 cGy $n = 4$, 0 cGy + PLX $n = 1$, 50 cGy $n = 2$, 50 cGy + PLX $n = 4$, 100 cGy $n = 0$; females: 0 cGy $n = 3$, 0 cGy + PLX $n = 1$, 50 cGy $n = 0$, 50 cGy + PLX $n = 2$, 100 cGy $n = 7$).

Calculated readouts for NOR included (for the first 3 and 5 min of testing) (i) interaction time with novel object (%) ((time of nose interaction with novel object)/(total time of nose interaction with novel object + familiar object)) × 100, (ii) interaction time with familiar object (%) ((time of nose interaction with familiar object)/(total time of nose interaction with novel object + familiar object)) × 100,

and (iii) discrimination index = (time of nose interaction with novel object − time of nose interaction with familiar object)/(total time of nose interaction with novel object + familiar object).

Radial arm water maze

The RAWM was used ~5 to 5.5 months after GCRsim to test spatial learning (*20*). The maze was a circular pool with a diameter of 118.5 cm and eight arms of 41 cm each in length. The pool was filled with water, and nontoxic white paint (54-2128-053, Crayola) was added to make the water opaque. An escape platform was placed at the end of one of the arms just below the surface of the water and hidden from view throughout the entire assay. Visual cues were placed around the room. Animals ran three consecutive 60-s trials with a 10-min intertrial interval. Animals were placed in an arm, not containing the escape platform, during each trial; the starting arm was changed each trial. If the animal successfully located the escape platform, they remained for 10 s and were then returned to the holding cage. If the animal was unable to locate the platform, the experimenter guided the animal to the escape platform, where they remained for 10 s before returning to the holding cage. The number of errors—entry into an arm without the escape platform—was determined using EthoVision software. The number of errors in trials 1 to 3 was averaged to calculate the "day average." Animals without whiskers, significant group outliers, and animals that died or did not swim in the pool were excluded from analysis (males: 0 cGy $n = 2$, 0 cGy + PLX $n = 2$, 50 cGy $n = 2$, 50 cGy + PLX $n = 4$, 100 cGy $n = 0$; females: 0 cGy $n = 3$, 0 cGy + PLX $n = 1$, 50 cGy $n = 1$, 50 cGy + PLX $n = 1$, 100 cGy $n = 7$).

Tissue collection

Seven days after GCRsim exposure, upon arrival at UCSF, blood was collected via the tail vein puncture in awake animals. Using a restrainer, a small nick was made in the tail vein using a scalpel and ~50 μl of blood was removed using a pipette and placed in a tube containing EDTA (Sigma-Aldrich). Blood was used to measure acute changes in peripheral blood biomarkers, discussed below.

Animals were lethally overdosed using a mixture of ketamine (10 mg/ml) and xylazine (1 mg/ml). Once animals were completely anesthetized, the chest cavity was opened. Mice were perfused with 1× phosphate-buffered saline (PBS) (pH 7.4) (Gibco) until the liver was clear (~1 to 2 min). Following PBS perfusion, the whole brain was quickly removed, and one hemisphere was immediately processed for microglia counts by flow cytometry. From the remaining hemisphere, brain regions were dissected (hippocampus), snap-frozen on dry ice, and stored at −80°C.

Flow cytometry

Blood

To assess circulating leukocyte populations, blood was aliquoted into tubes and stained with surface antibodies for 30 to 60 min at room temperature (*18*). Surface antibodies included anti-CD45 [fluorescein isothiocyanate (FITC)–conjugated; BD Biosciences], Ly6G [phycoerythrin (PE)–conjugated; BD Biosciences], CD8 (PE-Cy7–conjugated; BD Biosciences), CD4 [allophycocyanin (APC)–conjugated; BD Biosciences], and CD11b (APC-Cy7–conjugated; BD Biosciences). Leukocyte subpopulations were identified as follows: forward and side scatter was used to exclude debris and doublet populations. Specific T cell populations were identified as follows: CD4 T cell subsets were $CD4^+$, $CD45^+$, $Ly6G^-$, $CD8^-$, $CD11b^-$. CD8 T cell subsets were $CD8^+$, $CD45^+$, $Ly6G^-$, $CD4^-$, $CD11b^-$. Monocytes were $CD11b^+$, $CD45^+$, $Ly6G^-$, $CD4^-$, $CD8^-$. After surface antibody staining, red blood cells were lysed with RBC lysis (BD Biosciences). Data were collected on LSRII (BD Biosciences) and analyzed with FlowJo software (v10, Tree Star Inc.).

Synaptosomes

Snap-frozen hippocampi were homogenized using a glass Dounce homogenizer in 0.32 M sucrose in Hepes (H0887, Sigma-Aldrich, St. Louis, MO). Gross tissue fragments were removed by centrifugation (1200*g* for 10 min), and supernatant was collected. Synaptosomes were isolated by further centrifugation (13,000*g* for 20 min), pellets containing synaptosomes were collected, and supernatant was discarded. Synaptosome collection was standardized between samples using total protein concentration (Pierce BCA Protein Assay, 23225, Thermo Fisher Scientific, Rockford, IL). Synaptosomes (50 μg/ml) were divided into 1.5-ml microcentrifuge tubes for staining. For intracellular staining, synaptosomes were first permeabilized by Cytofix/Cytoperm fixation solution (554722, BD Biosciences, San Diego, CA) for 20 min. Samples were washed two times with 700 μl of perm/wash buffer (554723, BD Biosciences, San Diego, CA) at 13,000*g* for 5 min. Primary antibodies (synapsin-1, MAB1543, Millipore, Burlington, MA and PSD-95, ab13552, Abcam Cambridge, UK) were added for 30 min and agitated after 15 min. Samples were washed two times with 700 μl of perm/wash buffer at 13,000*g* for 5 min. Secondary antibodies (goat anti-rabbit 405, A31556, Invitrogen, Carlsbad, CA; goat anti-mouse 488 A11001, Invitrogen, Carlsbad, CA) were added for 30 min and agitated after 15 min in the dark. All reagents were made fresh for each staining day. Samples are kept cold (4°C, either on ice or in chilled centrifuges) for staining procedures. Synaptosomes were determined by size-calibrated beads and costaining with antibodies specific for pre-synaptic (synapsin-1) and post-synaptic (PSD-95) markers. No positive staining was observed in samples containing (i) no synaptosomes and (ii) secondary antibodies alone (*4*). A subset of 11 to 12 samples from each group was selected for flow synaptocytometry analysis. A maximum of three samples were processed per day. Each day, at least one 0 cGy sample was analyzed, and the 50 cGy and 50 cGy + PLX samples from the day were standardized to the 0 cGy group. Samples were run in triplicate. Data were collected on LSRII (BD Biosciences) and analyzed with FlowJo software (v10, Tree Star Inc.). Thirty thousand events were collected.

Microglia

Following perfusions, fresh brain hemispheres were cut into approximately 1-mm cubes with a razor blade and digested in 2 ml of cold Accutase in the presence of deoxyribonuclease I (DN25-100MG, Sigma-Aldrich) on ice with frequent pipetting for 20 min. A 70-μm cell strainer was used to remove large debris. Cells were collected by centrifugation and resuspended in 25% Percoll solution (P4937-100ML, Sigma-Aldrich) diluted in RPMI 1640 medium. After centrifuging at 800*g* for 20 min at 4°C, myelin debris and excess solutions were discarded. Cell pellet was then washed with fresh RPMI 1640 medium and resuspended in 100 μl of fluorescence-activated cell sorting (FACS) buffer [1 × Dulbecco's PBS (DPBS) with 0.5% bovine serum albumin (BSA) fraction V, 15260037 Gibco]. Cells were blocked with one volume of blocking solution [5% normal mouse serum, 5% normal rat serum, and 5% normal rabbit serum (015-000-120, 012-000-120, and 011-000-120, Jackson ImmunoResearch) and 2% fetal bovine serum (10082139, Gibco)] and 1% BSA fraction V × 1 DPBS for 30 min. Cells were then stained for 30 min with fluorophore-conjugated antibodies on ice (CD11b-AF700, 1:100 and

CD45-FITC, 1:50, 557690 and 553080, BD Pharmingen; C5aR-PE, 1:100, 130-106-174, Miltenyi Biotec). For intracellular staining, cells prestained with extracellular markers were fixed in 500 μl of fixation/permeabilization solution (554714, BD Biosciences) on ice for 15 min, washed twice with 1 × perm/wash buffer (554714, BD Biosciences), and stained with intracellular markers on ice for 30 min (CD107a-PE, 1:200, 130-102-219, Miltenyi Biotec; CD206-PE, 1:50, 141706, BioLegend). Stained cells were washed and resuspended in FACS buffer before analyses. Data were collected using an Aria III sorter (BD Biosciences) and analyzed with FlowJo software (v10, Tree Star Inc.). At least 3000 microglia events ($CD11b^{+}CD45^{low}$) were collected from each brain for fluorescence intensity comparisons. Because of limitations in how many individual animal flow stainings could be run each day, individual mean fluorescence intensity (MFI) values were standardized to sex-matched 0 cGy group for each day that flow was run (0 cGy, 50 cGy, and 50 cGy + PLX animals were equally divided on termination days).

Data analysis

Data are expressed as means ± SEM. Statistical analyses were performed as listed below, with P values of <0.05 considered as significant. Student's t test and one-, two-, and three-way ANOVAs were used. Individual statistical analysis is denoted in the figure legends. For RAWM, two-way repeated-measures ANOVA was used.

The number of mice used was sufficient to result in statistically significant differences using standard power calculations with $\alpha = 0.05$ and a power of 0.8. We used an online tool (http://bu.edu/orccommittees/iacuc/policies-and-guidelines/sample-size-calculations/) to calculate power and samples size based on experience with the respective tests, variability of the assays, and interindividual differences within groups. All experiments were randomized and blinded by an independent researcher before treatment.

Biological replicates are measurements of biologically distinct animals/tissues/cells used to measure biological differences. Technical replicates are repeated measurements of the same animals/tissues/cells.

PCA was performed in an unsupervised spectral decomposition of the correlation matrix across measured end points (i.e., blind to manipulated variables: radiation condition, sex, and depletion therapy) (*21*). PCs were retained using the eigenvalue >1 rule, scree plot, and pc overdetermination based on the loading weights. Loading weights (equivalent to Pearson r coefficients) are represented by heatmaps rendered in R and were used to name the PCs (*25*). PC scores (equivalent to mean-centered standardized z scores) were calculated for each subject using the regression method (range, −1.0 to 1.0) on each of the retained PCs. Syndromic plots were performed using the R syndRomics package (*42*). PC naming was performed using loadings > |0.45|. All analyses were performed in IBM SPSS v.26 and R v.4.0.3.

SUPPLEMENTARY MATERIALS

Supplementary material for this article is available at https://science.org/doi/10.1126/sciadv.abg6702

View/request a protocol for this paper from *Bio-protocol*.

REFERENCES AND NOTES

1. R. A. Mewaldt, Galactic cosmic ray composition and energy spectra. *Adv. Space Res.* **14**, 737–747 (1994).
2. G. A. Nelson, Space radiation and human exposures, a primer. *Radiat. Res.* **185**, 349–358 (2016).
3. E. Cekanaviciute, S. Rosi, S. V. Costes, Central nervous system responses to simulated galactic cosmic rays. *Int. J. Mol. Sci.* **19**, 3669 (2018).
4. K. Krukowski, K. Grue, E. S. Frias, J. Pietrykowski, T. Jones, G. Nelson, S. Rosi, Female mice are protected from space radiation-induced maladaptive responses. *Brain Behav. Immun.* **74**, 106–120 (2018).
5. J. Raber, A. R. Allen, S. Sharma, B. Allen, S. Rosi, R. H. Olsen, M. J. Davis, M. Eiwaz, J. R. Fike, G. A. Nelson, Effects of proton and combined proton and (56)Fe radiation on the hippocampus. *Radiat. Res.* **185**, 20–30 (2016).
6. J. Raber, J. Yamazaki, E. R. S. Torres, N. Kirchoff, K. Stagaman, T. Sharpton, M. S. Turker, A. Kronenberg, Combined effects of three high-energy charged particle beams important for space flight on brain, behavioral and cognitive endpoints in B6D2F1 female and male mice. *Front. Physiol.* **10**, 179 (2019).
7. M. S. Paladini, X. Feng, K. Krukowski, S. Rosi, Microglia depletion and cognitive functions after brain injury: From trauma to galactic cosmic ray. *Neurosci. Lett.* **741**, 135462 (2021).
8. M. Prinz, S. Jung, J. Priller, Microglia biology: One century of evolving concepts. *Cell* **179**, 292–311 (2019).
9. K. Krukowski, X. Feng, M. S. Paladini, A. Chou, K. Sacramento, K. Grue, L. K. Riparip, T. Jones, M. Campbell-Beachler, G. Nelson, S. Rosi, Temporary microglia-depletion after cosmic radiation modifies phagocytic activity and prevents cognitive deficits. *Sci. Rep.* **8**, 7857 (2018).
10. V. K. Parihar, M. Maroso, A. Syage, B. D. Allen, M. C. Angulo, I. Soltesz, C. L. Limoli, Persistent nature of alterations in cognition and neuronal circuit excitability after exposure to simulated cosmic radiation in mice. *Exp. Neurol.* **305**, 44–55 (2018).
11. B. D. Allen, A. R. Syage, M. Maroso, A. A. D. Baddour, V. Luong, H. Minasyan, E. Giedzinski, B. L. West, I. Soltesz, C. L. Limoli, J. E. Baulch, M. M. Acharya, Mitigation of helium irradiation-induced brain injury by microglia depletion. *J. Neuroinflammation* **17**, 159 (2020).
12. R. Rola, K. Fishman, J. Baure, S. Rosi, K. R. Lamborn, A. Obenaus, G. A. Nelson, J. R. Fike, Hippocampal neurogenesis and neuroinflammation after cranial irradiation with (56)Fe particles. *Radiat. Res.* **169**, 626–632 (2008).
13. B. Liu, R. G. Hinshaw, K. X. le, M. A. Park, S. Wang, A. P. Belanger, S. Dubey, J. L. Frost, Q. Shi, P. Holton, L. Trojanczyk, V. Reiser, P. A. Jones, W. Trigg, M. F. di Carli, P. Lorello, B. J. Caldarone, J. P. Williams, M. K. O'Banion, C. A. Lemere, Space-like 56Fe irradiation manifests mild, early sex-specific behavioral and neuropathological changes in wildtype and Alzheimer's-like transgenic mice. *Sci. Rep.* **9**, 12118 (2019).
14. V. K. Parihar, B. D. Allen, C. Caressi, S. Kwok, E. Chu, K. K. Tran, N. N. Chmielewski, E. Giedzinski, M. M. Acharya, R. A. Britten, J. E. Baulch, C. L. Limoli, Cosmic radiation exposure and persistent cognitive dysfunction. *Sci. Rep.* **6**, 34774 (2016).
15. L. C. Simonsen, T. C. Slaba, P. Guida, A. Rusek, NASA's first ground-based Galactic Cosmic Ray Simulator: Enabling a new era in space radiobiology research. *PLOS Biol.* **18**, e3000669 (2020).
16. R. G. Lister, The use of a plus-maze to measure anxiety in the mouse. *Psychopharmacology* **92**, 180–185 (1987).
17. M. Yang, J. L. Silverman, J. N. Crawley, Automated three-chambered social approach task for mice. *Curr. Protoc. Neurosci.* **56**, 8.26.1–8.26.16 (2011).
18. K. Krukowski, T. Jones, M. Campbell-Beachler, G. Nelson, S. Rosi, Peripheral T cells as a biomarker for oxygen-ion-radiation-induced social impairments. *Radiat. Res.* **190**, 186–193 (2018).
19. D. G. Mumby, S. Gaskin, M. J. Glenn, T. E. Schramek, H. Lehmann, Hippocampal damage and exploratory preferences in rats: Memory for objects, places, and contexts. *Learn. Mem.* **9**, 49–57 (2002).
20. J. Alamed, D. M. Wilcock, D. M. Diamond, M. N. Gordon, D. Morgan, Two-day radial-arm water maze learning and memory task; robust resolution of amyloid-related memory deficits in transgenic mice. *Nat. Protoc.* **1**, 1671–1679 (2006).
21. J. Haefeli, A. R. Ferguson, D. Bingham, A. Orr, S. J. Won, T. I. Lam, J. Shi, S. Hawley, J. Liu, R. A. Swanson, S. M. Massa, A data-driven approach for evaluating multi-modal therapy in traumatic brain injury. *Sci. Rep.* **7**, 42474 (2017).
22. N. N. Dagher, A. R. Najafi, K. M. N. Kayala, M. R. P. Elmore, T. E. White, R. Medeiros, B. L. West, K. N. Green, Colony-stimulating factor 1 receptor inhibition prevents microglial plaque association and improves cognition in 3xTg-AD mice. *J. Neuroinflammation* **12**, 139 (2015).
23. M. R. Elmore, A. R. Najafi, M. A. Koike, N. N. Dagher, E. E. Spangenberg, R. A. Rice, M. Kitazawa, B. Matusow, H. Nguyen, B. L. West, K. N. Green, Colony-stimulating factor 1 receptor signaling is necessary for microglia viability, unmasking a microglia progenitor cell in the adult brain. *Neuron* **82**, 380–397 (2014).
24. D. K. Wilton, L. Dissing-Olesen, B. Stevens, Neuron-glia signaling in synapse elimination. *Annu. Rev. Neurosci.* **42**, 107–127 (2019).
25. A. R. Ferguson, K. A. Irvine, J. C. Gensel, J. L. Nielson, A. Lin, J. Ly, M. R. Segal, R. R. Ratan, J. C. Bresnahan, M. S. Beattie, Derivation of multivariate syndromic outcome metrics for consistent testing across multiple models of cervical spinal cord injury in rats. *PLOS ONE* **8**, e59712 (2013).
26. J. D. Cherry, B. Liu, J. L. Frost, C. A. Lemere, J. P. Williams, J. A. Olschowka, M. K. O'Banion, Galactic cosmic radiation leads to cognitive impairment and increased Aβ plaque accumulation in a mouse model of Alzheimer's disease. *PLOS ONE* **7**, e53275 (2012).

27. A. Mange, Y. Cao, S. Zhang, R. D. Hienz, C. M. Davis, Whole-body Oxygen (16O) ion-exposure-induced impairments in social odor recognition memory in rats are dose and time dependent. *Radiat. Res.* **189**, 292–299 (2018).
28. C. B. Jones, A. Mange, L. Granata, B. Johnson, R. D. Hienz, C. M. Davis, Short and long-term changes in social odor recognition and plasma cytokine levels following oxygen (^{16}O) ion radiation exposure. *Int. J. Mol. Sci.* **20**, 339 (2019).
29. Z. S. Patel, T. J. Brunstetter, W. J. Tarver, A. M. Whitmire, S. R. Zwart, S. M. Smith, J. L. Huff, Red risks for a journey to the red planet: The highest priority human health risks for a mission to Mars. *NPJ Microgravity* **6**, 33 (2020).
30. G. Sonnenfeld, J. S. Butel, W. T. Shearer, Effects of the space flight environment on the immune system. *Rev. Environ. Health* **18**, 1–18 (2003).
31. J. Chang, Y. Luo, Y. Wang, R. Pathak, V. Sridharan, T. Jones, X. W. Mao, G. Nelson, M. Boerma, M. Hauer-Jensen, D. Zhou, L. Shao, Low doses of oxygen ion irradiation cause acute damage to hematopoietic cells in mice. *PLOS ONE* **11**, e0158097 (2016).
32. J. K. Sanzari, K. A. Cengel, X. S. Wan, A. Rusek, A. R. Kennedy, Acute hematological effects in mice exposed to the expected doses, dose-rates, and energies of solar particle event-like proton radiation. *Life Sci. Space Res.* **2**, 86–91 (2014).
33. D. S. Gridley, A. Obenaus, T. A. Bateman, M. J. Pecaut, Long-term changes in rat hematopoietic and other physiological systems after high-energy iron ion irradiation. *Int. J. Radiat. Biol.* **84**, 549–559 (2008).
34. C. O. Wambi, J. K. Sanzari, C. M. Sayers, M. Nuth, Z. Zhou, J. Davis, N. Finnberg, J. S. Lewis-Wambi, J. H. Ware, W. S. el-Deiry, A. R. Kennedy, Protective effects of dietary antioxidants on proton total-body irradiation-mediated hematopoietic cell and animal survival. *Radiat. Res.* **172**, 175–186 (2009).
35. J. H. Ware, J. Sanzari, S. Avery, C. Sayers, G. Krigsfeld, M. Nuth, X. S. Wan, A. Rusek, A. R. Kennedy, Effects of proton radiation dose, dose rate and dose fractionation on hematopoietic cells in mice. *Radiat. Res.* **174**, 325–330 (2010).
36. K. Krukowski, A. Chou, X. Feng, B. Tiret, M. S. Paladini, L. K. Riparip, M. Chaumeil, C. Lemere, S. Rosi, Traumatic brain injury in aged mice induces chronic microglia activation, synapse loss, and complement-dependent memory deficits. *Int. J. Mol. Sci.* **19**, 3753 (2018).
37. C. W. Hui, H. A. Vecchiarelli, É. Gervais, X. Luo, F. Michaud, L. Scheefhals, K. Bisht, K. Sharma, L. Topolnik, M. È. Tremblay, Sex differences of microglia and synapses in the hippocampal dentate gyrus of adult mouse offspring exposed to maternal immune activation. *Front. Cell. Neurosci.* **14**, 558181 (2020).
38. J. Raber, E. Rudobeck, M. Campbell-Beachler, A. R. Allen, B. Allen, S. Rosi, G. A. Nelson, S. Ramachandran, J. Turner, J. R. Fike, R. Vlkolinsky, (28)Silicon radiation-induced enhancement of synaptic plasticity in the hippocampus of naive and cognitively tested mice. *Radiat. Res.* **181**, 362–368 (2014).
39. X. W. Mao, C. J. Favre, J. R. Fike, L. Kubinova, E. Anderson, M. Campbell-Beachler, T. Jones, A. Smith, S. Rightnar, G. A. Nelson, High-LET radiation-induced response of microvessels in the hippocampus. *Radiat. Res.* **173**, 486–493 (2010).
40. D. I. Lowenstein, A. Rusek, Technical developments at the NASA Space Radiation Laboratory. *Radiat. Environ. Biophys.* **46**, 91–94 (2007).
41. J. W. Norbury, W. Schimmerling, T. C. Slaba, E. I. Azzam, F. F. Badavi, G. Baiocco, E. Benton, V. Bindi, E. A. Blakely, S. R. Blattnig, D. A. Boothman, T. B. Borak, R. A. Britten, S. Curtis, M. Dingfelder, M. Durante, W. S. Dynan, A. J. Eisch, S. Robin Elgart, D. T. Goodhead, P. M. Guida, L. H. Heilbronn, C. E. Hellweg, J. L. Huff, A. Kronenberg, C. la Tessa, D. I. Lowenstein, J. Miller, T. Morita, L. Narici, G. A. Nelson, R. B. Norman, A. Ottolenghi, Z. S. Patel, G. Reitz, A. Rusek, A. S. Schreurs, L. A. Scott-Carnell, E. Semones, J. W. Shay, V. A. Shurshakov, L. Sihver, L. C. Simonsen, M. D. Story, M. S. Turker, Y. Uchihori, J. Williams, C. J. Zeitlin, Galactic cosmic ray simulation at the NASA Space Radiation Laboratory. *Life Sci. Space Res.* **8**, 38–51 (2016).
42. A. Torres Espin, A. Chou, J. R. Huie, N. Kyritsis, P. S. Upadhyayula, A. R. Ferguson, Reproducible analysis of disease space via principal components using the novel R package syndRomics. *eLife* **10**, e61812 (2021).

Acknowledgments: We wish to thank P. Guida, A. Rusek, D. Schneider, M. Petry, C. Baran, and other NSRL physics and animal staff for help. A special thanks to A. Gray, D. Mabunga, J. Wilkerson, and K. Lindstrom for assistance with animal cohorts. A. Chou's and A. Torres Espin's expertise in figure compilation was greatly appreciated. The San Francisco General Hospital Flow Core Facility is supported by the NIH (P30 AI027763). Timelines and graphical abstract were made with BioRender.com. We also thank in-kind support from Data Robot Inc. and Scientific Advisory Panel, Neuronasal Inc. **Funding:** This work was supported by NASA grants NNX14AC94G (S.R.) and 80NSSC19K1581 (S.R.). E.S.F. is supported by the National Institute for General Medicine (NIGMS) Initiative for Maximizing Student Development (R25GM056847) and the NSF Graduate Fellowship Program. A.H. was supported by the UCSF Summer Research Training Program. E.E. was supported by the Sally Casanova Pre-Doctoral Scholarship. NIH/NINDS: R01NS088475 (A.R.F.) and UG3NS106899 (A.R.F.); Department of Veterans Affairs: 1I01RX002245 (A.R.F.) and I01RX002787 (A.R.F.); Wings for Life and Craig H. Neilsen Foundation (A.R.F.). **Author contributions:** Experimental and conceptual design (K.K., G.N., and S.R.); experimental implementation (K.K., K.G., M.B., E.E., E.S.F., X.F., T.J., and G.N.); data analysis (K.K., K.G., M.B., E.E., E.S.F., A.H., M.K.-Z., V.F., and H.N.); statistical analysis (K.K. and A.R.F.); manuscript preparation (K.K., K.G., M.B., A.R.F., G.N., and S.R.); final manuscript approval (K.K., K.G., M.B., E.E., E.S.F., A.H., M.K.-Z., V.F., S.N., X.F., G.N., A.R.F., and S.R.). **Competing interests:** The authors declare that they have no competing interests. **Data and materials availability:** All data needed to evaluate the conclusions in the paper are present in the paper and/or the Supplementary Materials. Raw datasets are available at https://doi.org/10.7272/Q63J3B6G.

Submitted 20 January 2021
Accepted 20 August 2021
Published 15 October 2021
10.1126/sciadv.abg6702

Citation: K. Krukowski, K. Grue, M. Becker, E. Elizarraras, E. S. Frias, A. Halvorsen, M. Koenig-Zanoff, V. Frattini, H. Nimmagadda, X. Feng, T. Jones, G. Nelson, A. R. Ferguson, S. Rosi, The impact of deep space radiation on cognitive performance: From biological sex to biomarkers to countermeasures. *Sci. Adv.* **7**, eabg6702 (2021).